Journal of Sound and Vibration (2002) **256**(5), 803–820
doi:10.1006/jsvi.5020, available online at http://www.idealibrary.com on IDEAL®

APPLICATION OF NON-SMOOTH MODELLING TECHNIQUES TO THE DYNAMICS OF A FLEXIBLE IMPACTING BEAM

D. J. WAGG

Department of Mechanical Engineering, University of Bristol, Queens Building, University Walk, Bristol BS8 1TR, England. E-mail: david.wagg@bristol.ac.uk

AND

S. R. BISHOP

Centre for Nonlinear Dynamics and its Applications University, College London, Gower Street, London WC1E 6BT, England

(*Received* 2 *April* 2001, *and in final form* 14 *January* 2002)

Non-smooth modelling techniques have been successfully applied to lumped mass-type structures for modelling phenomena such as vibro-impact and friction oscillators. In this paper, the application of these techniques to continuous elements using the example of a cantilever beam is considered. Employing a Galerkin reduction to form an N-degree-of-freedom modal model, a technique for modelling impact phenomena using a non-smooth dynamics approach is demonstrated. Numerical simulations computed using the non-smooth model are compared with experimentally recorded data for a flexible beam constrained to impact on one side. A method for dealing with sticking motions when numerically simulating the beam motion is presented. In addition, choosing the dimension of the model based on power spectra of experimentally recorded time series is discussed.

1. INTRODUCTION

In this paper, the dynamics of a flexible vibro-impacting cantilever beam system is considered. Such continuous beam systems, even without impacts, have well-known multi-modal behaviour which has been documented in a number of classic texts [1–3]. The problem of a cantilever beam impacting against an impact stop has also been considered by several authors, see for example references [4, 5] and the references therein. However, in general, this latter body of literature has been concerned mainly with modelling the impact event itself, rather than the global dynamics of the beam.

Following the work of Moon and Holmes [6] and Moon and Shaw [7], a new approach to modelling the vibro-impact dynamics of beams has been developed [8–10]. In this approach, the beam is modelled as a single-degree-of-freedom system, and a piecewise linear stiffness or coefficient of restitution rule is used to model the impact process. For example, Moon and Holmes [6] considered the non-linear dynamics of a beam subject to harmonic and magnetic forcing, using a Galerkin method to reduce the system to a single-degree-of-freedom (see also reference [11]). Moon and Shaw [7] and Shaw [8] considered a single-degree-of-freedom approach to modelling a vibro-impact cantilever beam

0022-460X/02/$35.00

experiment, also by reducing the model to a single mode. In this case, the system was considered as piecewise linear, and the single-degree-of-freedom model was obtained using a Galerkin method applied to each linear part. Also, using a single-degree-of-freedom approach to model beam dynamics Bishop *et al.* [9] compared experimental and numerical results for a stiff vibro-impact cantilever beam by using an instantaneous coefficient of restitution model for the impacts.

A similar coefficient of restitution rule is used in combination with a single-degree-of-freedom linear oscillator to form the now well-known impact oscillator [12]. These systems have non-smooth dynamical characteristics which have been studied in depth in recent years; see for example references [13–18] and references therein. Other approaches to modelling multi-dimensional impact oscillators have included the use of non-smooth mappings [19], finite elements [20] and studies of lumped mass-type systems [21–25]. In addition, work on estimating the dimension of multi-dimensional impact oscillators has been carried out by Cusamano *et al.* [26] using correlation dimension, and by Azeez and Vakakis [27], who consider proper orthogonal decomposition as a means of both estimating dimension and creating a low-dimensional model of a flexible vibro-impact system. Other authors have studied vibro-impact systems which include continuous rods [28, 29] and beam elements [30–32].

In this paper, the problem of modelling flexible beams subject to impacts, which because of their flexibility require multiple modes to capture adequately their dynamical behaviour, is addressed. In common with previous studies, a Galerkin approach is used to reduce the system to a finite set of ordinary differential equations—previously usually one. However, in this work a technique is presented which allows more than a single mode to be used in the model. In order to model the impact process, a non-smooth model based on the instantaneous coefficient of restitution rule is used. Qualitative comparisons with experimental results using models with one to four degrees of freedom will be presented, and the issues of chatter, sticking and choosing the dimension of the model are discussed in detail. Finally, comparisons between experimentally recorded and numerically computed bifurcation diagrams will be drawn.

2. EQUATIONS OF MOTION

Consider a vertically clamped cantilever beam with a motion limiting constraint on one side. This scenario is shown in Figure 1, where the beam is constrained by an impact stop at a single point. The stop is positioned at a distance B from the base along the beam, and with an initial transverse distance a from the beam. It is assumed that the beam is harmonically forced at a distance C from the base because this relates to the situation in the experimental system which will be discussed in section 4.

The transverse vibration of the centreline of the beam is denoted by $u(x, t)$, where x is the length along the beam from the base and t is the time. It is assumed that the beam vibrates with small enough displacements such that it remains within the linear elastic range. Therefore, a classical approach can be used for deriving the equation of motion (for example reference [3]), such that the equation of motion for the beam away from the impact constraint can be written as

$$\frac{EI}{L^4}\frac{\partial^4 u}{\partial s^4} + \eta\frac{\partial u}{\partial t} + \rho A\frac{\partial^2 u}{\partial t^2} = f(s, t) \quad u < a, \tag{1}$$

where E is the Young's modulus, ρ the density, A the cross-sectional area and I the second moment of area for the beam of length L. As a measure of length along the beam centreline

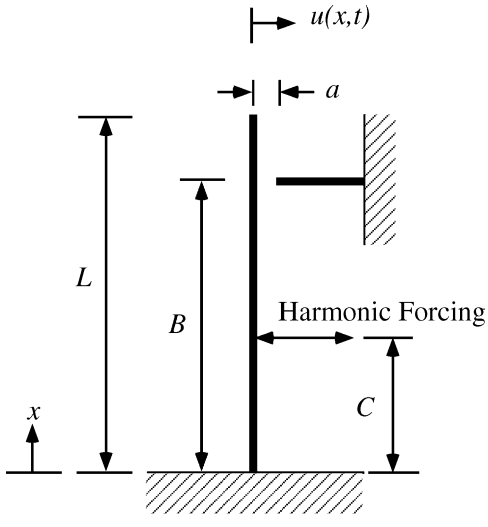

Figure 1. Schematic representation of a continuous vibro-impact cantilever beam system.

the non-dimensional co-ordinate $s = x/L$ is defined, such that the distance along the beam $s \in [0, 1]$, and the function $f(s, t)$ represents the forcing of the beam per unit length. Similarly, $b = B/L$ and $c = C/L$. In addition, the beam has viscous damping, η, per unit length. Equation (1) is the Euler–Bernoulli beam equation for a beam with viscous damping and forcing. In the following analysis, ρ, A and I are considered to be constant, corresponding to the case of a beam with uniform cross-section throughout its length.

2.1. NON-SMOOTH IMPACT CONDITION

When an impact occurs $u(b, t) = a$ and a coefficient of restitution rule of the form

$$\dot{u}(b, t_+) = -r\dot{u}(b, t_-), \quad u(b, t_-) = a \tag{2}$$

is applied, where t_- is the time just before impact, t_+ is the time just after impact and $r \in [0, 1]$ is a coefficient of restitution. It is assumed that the velocities, $\dot{u}$ are normal to the beam centreline, and that the tangential velocity component at impact is negligible.

For systems with steel impacting components, it has been demonstrated the cumulative impact time can be as little as 1% of the overall time [33]. Thus, for this class of systems it can be assumed that the time of contact for individual impacts is so small as to be close to zero. This assumption means that equation (2) can be applied instantaneously such that $t_- = t_+$, and a non-smooth discontinuity in velocity occurs at impact. The advantage of using this assumption is that the analysis of the system is simplified as there is no need to compute the time of impact.

However, previous systems studied using this non-smooth assumption have been the lumped mass type. For such systems, the velocity vector relates to a set of discrete lumped masses. Thus, a particular lumped mass can have a non-smooth discontinuity in its velocity field independently from the other masses. For a continuous structural element, such as a beam, the velocity is a continuous function of beam length. Thus, in order to apply the non-smooth impact condition (equation (2)), at $u = a$, the velocity components for the

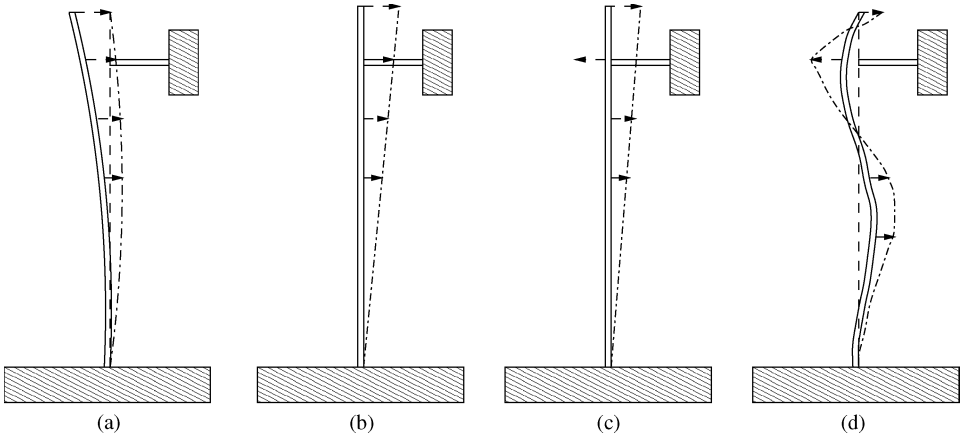

Figure 2. Schematic representation of a continuous cantilever beam: (a) before impact, (b) at time $t = t_-$, (c) at time $t = t_+$, and (d) after impact. Note: for simplicity $a = 0$ in this figure.

non-impacting part of the beam $s \neq b$ remain unaffected. Therefore in addition to equation (2), the relation

$$\dot{u}(s \neq b, t_+) = \dot{u}(s \neq b, t_-), \quad u(b, t_-) = a \tag{3}$$

also applies.

The combination of equations (2) and (3) are essentially a non-smooth representation of the physical impact process for the beam. In the physical beam system, the contact time will be finite (though small for materials with high stiffness) and the velocity reversal will propagate outwards from the point of impact, a process which is captured with this type of model.

The application of this type of non-smooth impact law to a continuous beam can be illustrated using the schematic diagrams shown in Figure 2. In Figure 2(a) the beam is away from impact, but with a velocity field, indicated with arrows, is acting in a direction which is forcing the beam towards the impact stop. Figure 2(b) represents the time $t = t_-$, which is the first part of the non-smooth impact process; the beam has come into contact with the stop, $u = a$ at time $t = t_-$, just before the application of the coefficient of restitution rule. The next stage in the impact process is the application of the coefficient of restitution rule at time $t = t_+$, shown in Figure 2(c), where the velocity at the point of contact has been reversed and reduced. Finally, the beam leaves contact with the stop (Figure 2(d)) with time $t > t_+$. Figure 2(d) also shows the case where the velocity field for the beam has both positive and negative components at the same time.

So, after an impact has occurred it is possible for some parts of the beam to be moving away from the impact stop, and at the same time other parts of the beam are still moving towards the impact stop. This type of behaviour has been observed qualitatively during experimental testing of vibro-impacting flexible beam systems. The aim here is to use the non-smooth impact conditions for the beam, equations (2) and (3), combined with multi-modal modelling techniques to obtain a continuous non-smooth model of such flexible beam systems.

2.2. GALERKIN REDUCTION

The Euler–Bernoulli equation can be reduced to a series of ordinary differential equations by using the standard Galerkin approach (see for example reference [34]), such

that the transverse displacement of the beam is approximated by

$$u(s, t) = \sum_{j=1}^{\infty} \phi_j(s)\, q_j(t), \tag{4}$$

where $\phi_j(s)$ are the normal mode shapes of the beam, and $q_j(t)$ are the modal co-ordinates. Then, by substituting equation (4) into the Euler–Bernoulli equation (equation (1)), applying the orthogonality principle for normal modes [3], and then truncating to N equations yields

$$\sum_{j=1}^{N} \left(\omega_{nj}^2 q_j(t) + 2\zeta_j \omega_{nj} \dot{q}_j(t) + \ddot{q}_j(t) = \frac{1}{\rho A} \int_0^1 f(s, t)\ \phi_j \, \mathrm{d}s \right) \quad j = 1, 2, 3 \ldots N, \tag{5}$$

where the natural frequency of each mode is

$$\omega_{nj} = (\xi_j)^2 \sqrt{\frac{EI}{\rho A L^4}} \tag{6}$$

and ξ_j is the jth eigenvalue. A further assumption is that damping η is linearly proportional to stiffness where $\zeta_j = \eta/\eta_c$ is the ratio of damping to critical damping $\eta_c = 2\rho A \omega_{nj}$.

It is assumed that $f(s, t)$ can separated into a space-dependent function and a time-dependent function such that $f(s, t) = g(s)\, h(t)$. Therefore, as the forcing is applied at a single point, $s = c$, $g(s)$ is a Dirac delta function $g(s) = \delta(s - c)$. Thus, the integral term in equation (5) becomes

$$\int_0^1 f(s, t)\, \phi_j \, \mathrm{d}s = h(t) \int_0^1 \delta(s - c/L)\, \phi_j \, \mathrm{d}s = h(t)\, \phi_i(c/L) = h(t)\, \alpha_j, \tag{7}$$

where α_j is a constant value for each mode, dependent only on the predefined position of forcing at $s = c$. Note that when c is close to a node point for a particular mode, the excitation of this mode can be significantly reduced, because $\phi_j = 0$ at a node point. Conversely, if c is at an anti-node, then the excitation of that mode will be maximized.

For each mode, the equation governing the modal co-ordinate is then

$$\ddot{q}_j(t) + 2\zeta_j \omega_{nj} \dot{q}_j(t) + \omega_{nj}^2 q_j(t) = \frac{\alpha_j}{m} h(t), \tag{8}$$

where $m = \rho A L$. Equation (8) has a well-known exact solution (see for example reference [3]) which applies during non-impacting motion, $u(b, t) < a$.

2.3. MODE SHAPES AND INITIAL CONDITIONS

In previous studies of the constrained cantilever beam, Moon and Shaw [7] and Shaw [8], the solution of a clamped–free cantilever is matched with a clamped–pinned beam at impact to obtain a solution for a piecewise linear beam model. This approach is based on the assumption that the beam is in contact with the stop for some contact time t_c and that only a single mode of vibration is considered. Our current approach is to use a non-smooth coefficient of restitution rule (equations (2) and (3)) for which t_c is assumed to be so short as to be approximately equal to zero. Thus, when an impact occurs, the beam is in contact with the constraint for a negligible (ideally zero) amount of time, and as a result mode shapes of

the beam during impact are not considered to be those of a clamped–pinned beam (see discussion on sticking in section 5.1).

The normal modes shapes for a cantilever beam can be defined as

$$\phi_j(s) = (\cosh \xi_j s - \cos \xi_j s) - \sigma_j(\sinh \xi_j s - \sin \xi_j s), \quad j = 1, 2, 3, \ldots \tag{9}$$

where

$$\sigma_j = \frac{(\sinh \xi_j - \sin \xi_j)}{(\cosh \xi_j + \cos \xi_j)} \tag{10}$$

and ξ_j are the eigenvalues of the beam [35].

If required, the initial conditions for the motion of the beam can be determined from

$$u(s, 0) = \sum_{j=1}^{\infty} \phi_j(s)\, q_j(0) \tag{11}$$

and

$$\dot{u}(s, 0) = \sum_{j=1}^{\infty} \phi_j(s)\, \dot{q}_j(0). \tag{12}$$

In all the simulations and experiments in this current work, the initial conditions are $u(s, 0) = \dot{u}(s, 0) = 0$.

3. VIBRO-IMPACT CANTILEVER BEAM ANALYSIS

In this section, a non-smooth model for a vibro-impacting continuous beam is obtained by combining the non-smooth impact law with a Galerkin reduction of the Euler–Bernoulli equation. Firstly, following the standard Galerkin approach, the number of modes is truncated to N, such that the dynamics of the beam is modelled by N ordinary differential equations of the form of equation (8). The condition for an impact to occur is that $u(b, t) = a$, and as the systems is now truncated to a set of N modes, the condition for impact can be written as

$$u(b, t) = a = \sum_{j=1}^{N} \phi_j(b)\, q_j(t) = \boldsymbol{\phi}(b)\, \mathbf{q}(t), \tag{13}$$

where $\boldsymbol{\phi}(b) = [\phi_1(b), \phi_2(b), \ldots, \phi_N(b)]$ and $\mathbf{q}(t) = [q_1(t), q_2(t), \ldots, q_N(t)]^{\mathrm{T}}$. Using this relationship in the impact law, equation (2) can be expressed as

$$\boldsymbol{\phi}(b)\, \mathbf{q}(t_+) = -r\boldsymbol{\phi}(b)\, \mathbf{q}(t_-), \quad \boldsymbol{\phi}(b)\, \mathbf{q}(t) = a. \tag{14}$$

In the $N = 1$, cases $\boldsymbol{\phi}(b)$ and $\mathbf{q}(t)$ become scalar and the relationship reduces to $\mathbf{q}(t_+) = -r\mathbf{q}(t_-)$. However, for $N > 1$ this cannot hold because for the remainder of of the beam, $s \neq b$, equation (3) applies during impact.

3.1. EXAMPLE: TWO-MODE MODEL OF BEAM

To demonstrate how to include the effect of equation (3) consider the case for $N = 2$, using the displacement of the beam at the point of impact, $s = b$ and the point of forcing,

$s = c$. Thus, for such a system at an impact

$$\begin{aligned} \dot{u}(b, t_+) &= -r\dot{u}(b, t_-), \\ \dot{u}(c, t_+) &= \dot{u}(c, t_-), \end{aligned} \tag{15}$$

which can be written as

$$\begin{aligned} \boldsymbol{\phi}(b)\,\dot{\mathbf{q}}(t_+) &= -r\boldsymbol{\phi}(b)\,\dot{\mathbf{q}}(t_-), \\ \boldsymbol{\phi}(c)\,\dot{\mathbf{q}}(t_+) &= \boldsymbol{\phi}(c)\,\dot{\mathbf{q}}(t_-), \end{aligned} \tag{16}$$

where, in this case $\boldsymbol{\phi}(b) = [\phi_1(b), \phi_2(b)]$, $\phi(c) = [\phi_1(c), \phi_2(c)]$ and $\dot{\mathbf{q}}(t) = [\dot{q}_1(t), \dot{q}_2(t)]^{\mathrm{T}}$. The relations in equation (16) can be combined to give

$$[\Phi]\,\dot{\mathbf{q}}(t_+) = [R][\boldsymbol{\Phi}]\,\dot{\mathbf{q}}(t_-), \tag{17}$$

where $[\boldsymbol{\Phi}] = [\boldsymbol{\phi}(b), \boldsymbol{\phi}(c)]^{\mathrm{T}}$ is a (2×2) matrix and

$$[\mathbf{R}] = \begin{bmatrix} -r & 0 \\ 0 & 1 \end{bmatrix} \tag{18}$$

is the coefficient of restitution matrix. Finally, from equation (17) a relationship for the modal velocities at impact is obtained,

$$\dot{\mathbf{q}}(t_+) = [\Phi]^{-1}[\mathbf{R}][\Phi]\,\dot{\mathbf{q}}(t_-), \tag{19}$$

which is a modal form of the coefficient of restitution rule.

The following observations on this example are made:

1. To have square matrices, this analysis requires that the number of modes N to be equal to the number of points considered on the beam. Square matrices simplify the analysis as matrices have to be inverted.
2. The matrix $[\Phi]$ is effectively a subset of the full modal matrix containing the normal modes for the beam. As N becomes larger, $[\Phi]$ becomes a better approximation of the full modal matrix.
3. For vibro-impact systems, the effect of decoupling the governing Euler–Bernoulli equation into normal mode components is to couple the modes via impact; equation (19).

This analysis can be generalized to consider any number of points along the beam. To ensure that square matrices are used, it is assumed that the number of modes, N, and the number of points along the beam are the same. Note also that this set of points must include the point of impact. Then the matrix $[\Phi]$ can be written as

$$[\Phi] = \begin{bmatrix} \phi_1(s_1) & \phi_2(s_1) & \dots & \phi_N(s_1) \\ \phi_1(s_2) & \phi_2(s_2) & \dots & \phi_N(s_2) \\ \phi_1(s_3) & \phi_2(s_3) & \dots & \phi_N(s_3) \\ \vdots & \vdots & \dots & \vdots \\ \phi_1(s_N) & \phi_2(s_N) & \dots & \phi_N(s_N) \end{bmatrix}. \tag{20}$$

and $[\mathbf{R}] = diag[1, 1, \dots, -r, \dots, 1, 1]$, with the coefficient of restitution positioned to coincide with the position of the impact stop.

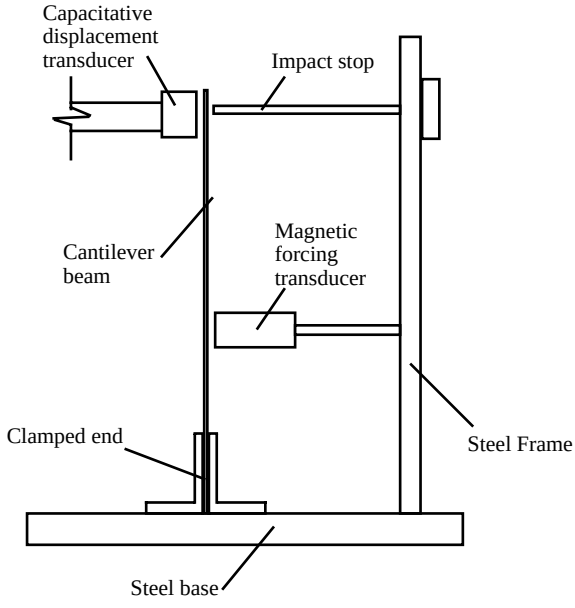

Figure 3. Schematic representation of the beam apparatus.

4. EXPERIMENTAL RESULTS

The experimental results were recorded from a steel cantilever beam apparatus constructed specifically for this work. A schematic representation of the experimental apparatus is shown in Figure 3. The cantilever beam has dimensions of length 300 mm width 25·5 mm and thickness 0·49 mm. The beam is clamped vertically into a steel base, to which a steel frame is attached which provides a housing for the impact stop, displacement and forcing transducers. The impact stop is a 3 mm diameter steel rod, with a rounded tip, fixed to the frame with a lock nut. The magnetic forcing transducer consists of an electro magnet capable of producing a variable magnetic field from an input analogue voltage signal which is provided via a LabPC + data acquisition card installed in a personal computer. The capacitative displacement transducer works in conjunction with a Wayne Kerr TE 100 Mk II feedback amplifier. The transducer is calibrated to read displacements in the range of $\pm 1{\cdot}25$ mm. The signal from the Wayne Kerr is recorded using the LabPC + card.

Using equation (6), the first four natural frequencies for the beam have been computed using the following parameter values. Young's Modulus $E = 205 \times 10^9$ N/m^2, second moment of area $I = 24{\cdot}4 \times 10^{-14}$ m^4, density $\rho = 8500$ kg/m^3, cross-sectional area $A = 12{\cdot}4 \times 10^{-6}$ m^2 and length $L = 0{\cdot}3$ m. The results are $f_1 = 4{\cdot}3$, $f_2 = 26{\cdot}84$, $f_3 = 75{\cdot}1$, $f_4 = 147{\cdot}3$, where $f_j = \omega_{nj}/2\pi$ Hz. These compare with measured frequencies (see Figures 4 and 5(b)) of $f_1 \approx 3{\cdot}8$ Hz, $f_2 \approx 21{\cdot}5$ Hz, $f_3 \approx 106$ Hz and $f_4 \approx 210$ Hz. From these measurements, it can be seen that the analytically computed frequency is a reasonably close approximation for f_1, but the accuracy of the predicted frequency decreases with increasing mode number.

A frequency response diagram for the beam is shown in Figure 4. For this and all subsequent figures, the convention of reference [36] is followed where the amplitude of response is shown in voltage units. From Figure 4 the shape of the resonance peaks indicate that the beam is lightly damped. The damping for the flexible beam was estimated using

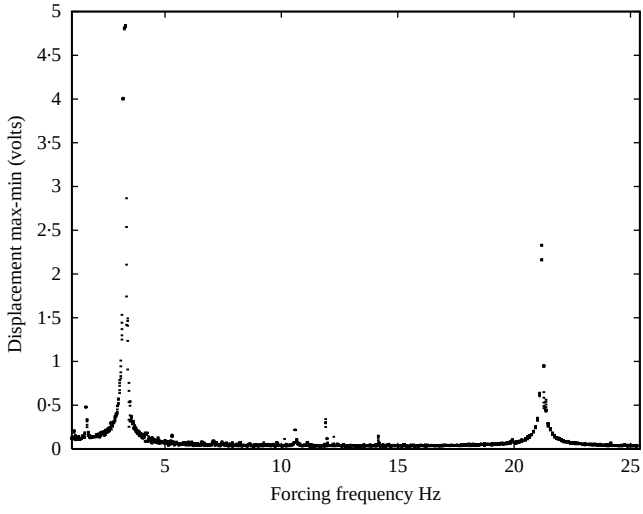

Figure 4. Experimentally recorded frequency-response diagram for the beam, showing first two resonance peaks. Maximum minus minimum displacement versus forcing frequency.

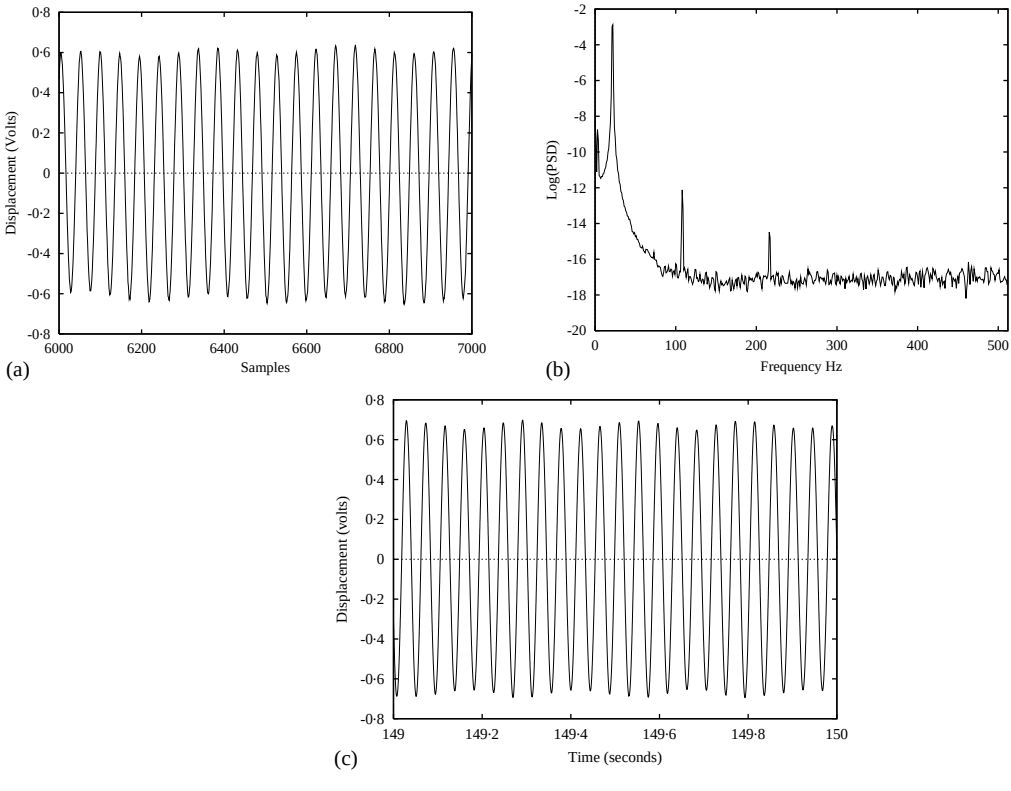

Figure 5. Experimentally recorded signal for the beam with a forcing frequency of $f = 21{\cdot}0$ Hz: (a) non-impacting time series sample rate 1000 samples/s, (b) power spectrum, (c) numerical simulation of non-impact motion in (a), parameter values; $F = 0{\cdot}6$(V), $\Omega = 144$, $N = 4$, $\eta = 0{\cdot}005$.

a half-power bandwidth on the first two resonance peaks to occur in the response spectrum corresponding to the first two natural frequencies of the beam. Using this frequency response data gives a value of η (including data from some free vibration tests) in the range 0·01–0·005 (Ns/m)/m. The value $\eta = 0{\cdot}005$ was subsequently used for all modes in the numerical simulations. If data could be obtained for more than the first two modes, it is anticipated that the accuracy of the model could be improved by including individual damping values for each mode. Each experimental test was started from the static state, so determining initial conditions for the experimental beam, was straightforward because $u(s, 0) = \dot{u}(s, 0) = 0, \forall s$.

In Figure 5(a) 1 s of a typical non-impacting time series sampled at a rate of 1000 samples per second from the flexible beam forced at $f = 21$ Hz (close to the second natural frequency) is shown. The power spectrum of this signal is shown in Figure 5(b). From the power spectrum, it can be seen that for the non-impacting response the most significant modal components are the first four, f_1, f_2, f_3 and f_4, and as the system is being forced close to f_2, this is the largest component in the response. In fact, it is not possible to distinguish any other modal contribution from noise above f_4 (approximately 210 Hz). Thus, by viewing the power spectrum for this particular beam time series the number of modes which contribute to the overall motion can be estimated, by the appearance of the associated modal frequency in the spectrum. This gives a basis for choosing N in the Galerkin approach developed in section 2.2.

Two other approaches have been discussed for estimating the number of modes to include in modelling continuous vibro-impacting systems. Cusamano *et al.* used a correlation dimension approach [26] and Azeez and Vakakis have demonstrated a method based on proper orthogonal decomposition [27].

5. NUMERICAL SIMULATION OF FLEXIBLE BEAM

Having chosen N, and estimated the parameters and initial conditions for the beam a numerical time series of the beam motion can be computed. This is achieved by computing the exact solution to equation (8) in small time steps Δt such that $t_{n+1} = t_n + \Delta t$, for each mode included in the model. This is by assuming that initially the beam starts away from the impact stop. At each time step, the condition $\phi(b)\,\mathbf{q}(t_n) < a$ is checked. When $\phi(b)\,\mathbf{q}(t_n) > a$, the values $\mathbf{q}(t_{n-1})$ and $\mathbf{q}(t_n)$ are on either side of the impact discontinuity, and a secant-type root finding method is used to compute the exact time of crossing t_i from which the modal values at impact $\mathbf{q}(t_i)$ are found. Then the impact law (equation (19)) is applied and the time stepping of the exact solutions continues.

5.1. STICKING MOTIONS

For some parameter values, the beam undergoes a succession of low-velocity impacts in quick succession. In impacting systems, this phenomenon is referred to as "chatter" [37]. If the sequence of low-velocity impacts continues, the beam can become stuck to the stop, in a similar way that a bouncing ball eventually comes to rest on a horizontal surface. For the beams considered in this study, the regions of chatter were very small, and periods of sticking behaviour were very short in comparison to the forcing periods. As a result, this behaviour could not be qualitatively observed experimentally due to limitations in the experimental sampling rate, but was observed in the numerical simulations of the beam.

A sticking motion typical of those observed during numerical simulation is shown in Figure 6. In Figure 6(a), a 2 s sample of a vibro-impact time series is shown, and in (b)

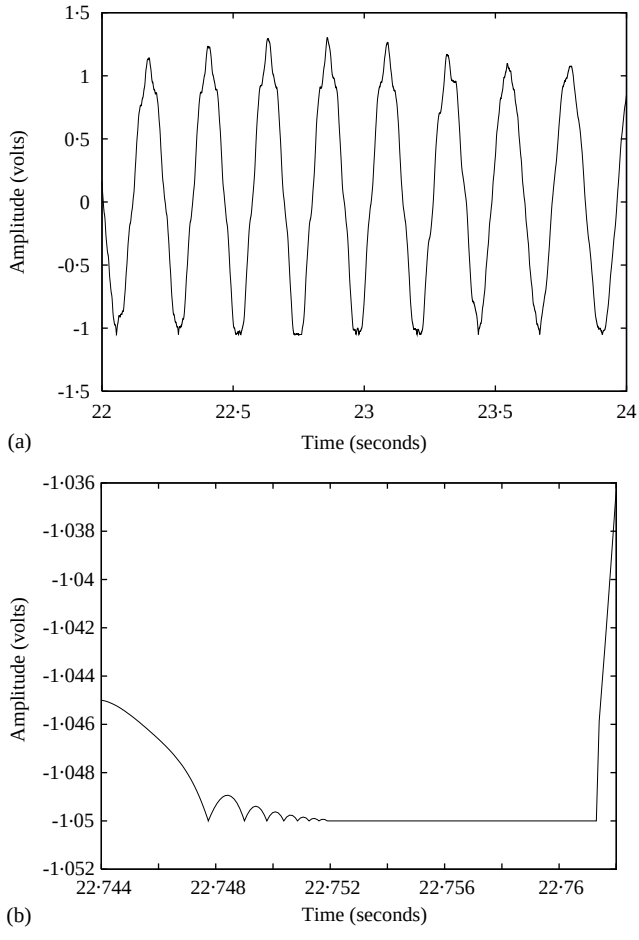

Figure 6. Numerical simulation of a typical sticking motion. Parameter values $a = -1{\cdot}05$, $r = 0{\cdot}8$, $F = 0{\cdot}1$, $N = 4$, $\rho = 8500$, $E = 2{\cdot}05 \times 10^{11}$, $\Omega = 27{\cdot}21$ and $\eta = 0{\cdot}005$. (a) Time series of motion with sticking close to $t = 22{\cdot}76$. (b) Close up around the sticking region.

a close up around the sticking region, which in this case occurs close to $t = 22{\cdot}76$. Here a succession of low-velocity impacts forming a chatter sequence followed by a short sticking period can be observed.

To deal with sticking motions numerically the approach proposed by Cusumano *et al.* [22] is adopted, which is based on recording the time interval between subsequent impacts. When this time interval falls below a certain threshold, as it can after a chatter sequence, the beam is assumed to be stuck to the stop. The method proposed by Cusumano *et al.* [22] was for a lumped mass system with a single mass subject to a motion limiting constraint. Once sticking had been detected the force holding the constrained mass against the stop could be computed from the motion of the remaining masses. When this force passed through zero, the mass will no longer be held against the stop and so the sticking motion ends.

For continuous systems this approach cannot be so easily applied, and for this study a different method has been applied. The onset of sticking is computed in the same way, by monitoring the time interval between successive impacts. Then during the sticking phase, a root finding method is used to compute the required force, applied at the point of impact,

to keep the beam displacement equal to the stop distance, i.e., $u(b, t_i) = a$. When this force passes through zero the sticking motion is deemed to have ended.

To model sticking motion, the approach of assuming that the beam is clamped–pinned during sticking [7, 8] was also considered. However, for systems where $N > 1$ this means that at impact

$$u(b, t) = \sum_{j=1}^{N} \phi_j(s)\, q_j = \sum_{j=1}^{N} \psi_j(s)\, q_j = a, \tag{21}$$

where $\psi_j(s)$ are the modes for a clamped–pinned beam. In general, this relation cannot hold as

$$\sum_{j=1}^{N} \phi_j(s)\, q_j \neq \sum_{j=1}^{N} \psi_j(s)\, q_j. \tag{22}$$

An alternative would be to use the relationship

$$u(b, t) = \sum_{j=1}^{N} \phi_j(s)\, q_j = \sum_{j=1}^{N} \psi_j(s)\, \hat{q}_j = a, \tag{23}$$

where $\hat{q}_j$ are the modal co-ordinates for a clamped–pinned beam. However, this leaves the problem of the relating the two sets of modal co-ordinates q_j and $\hat{q}_j$ at the point of discontinuity. Therefore, clamped–free modes were used during simulations of sticking motion.

5.2. COMPARISON BETWEEN NUMERICAL AND EXPERIMENTAL RESULTS

For comparison between numerical and experimental results, Figure 5(c) shows a simulation of the non-impact motion shown in Figure 5(a). This simulation (using a four-degree-of-freedom model) has been computed using the Galerkin method, with $N = 4$, and using a harmonic forcing function of the form $f(t) = F\cos(\Omega t)$. It can be seen from Figures 5(c) and 5(a) that there is good qualitative correlation, indicating that the modelling method works for the non-impacting case, a fact which is already well known from the general literature on classic vibration theory [1–3].

In Figure 7(a), a typical vibro-impact time series recorded from the flexible beam experiment at a forcing frequency of $\Omega = 20{\cdot}8$ Hz close to the second natural frequency is shown. The power spectrum of this motion is shown in Figure 7(c), here vertical lines represent the theoretically computed natural frequencies of the non-impacting beam. It is interesting to compare this power spectrum with the non-impact example in Figure 5(b). The vibro-impacting power spectrum has a much greater high-frequency content. In addition, there are several significant power spikes in the spectrum, and it is not obvious whether these are due to a modal contribution or could be attributed to the non-linearity in the system. For the first two computed natural frequencies, there does seem to be a reasonable correlation with a nearby power spike in the spectrum. The power spike at approximately 60 Hz may be due to the third mode, but from the three remaining spikes at 120, 160 and 195 Hz, it is not possible to distinguish which correlates to the fourth and fifth modal contributions. However, in common with the non-impacting case there is no significant modal contribution above 250 Hz. By comparison with Figure 5, it can be observed that the additional power spikes in the spectrum are due to the non-linearity

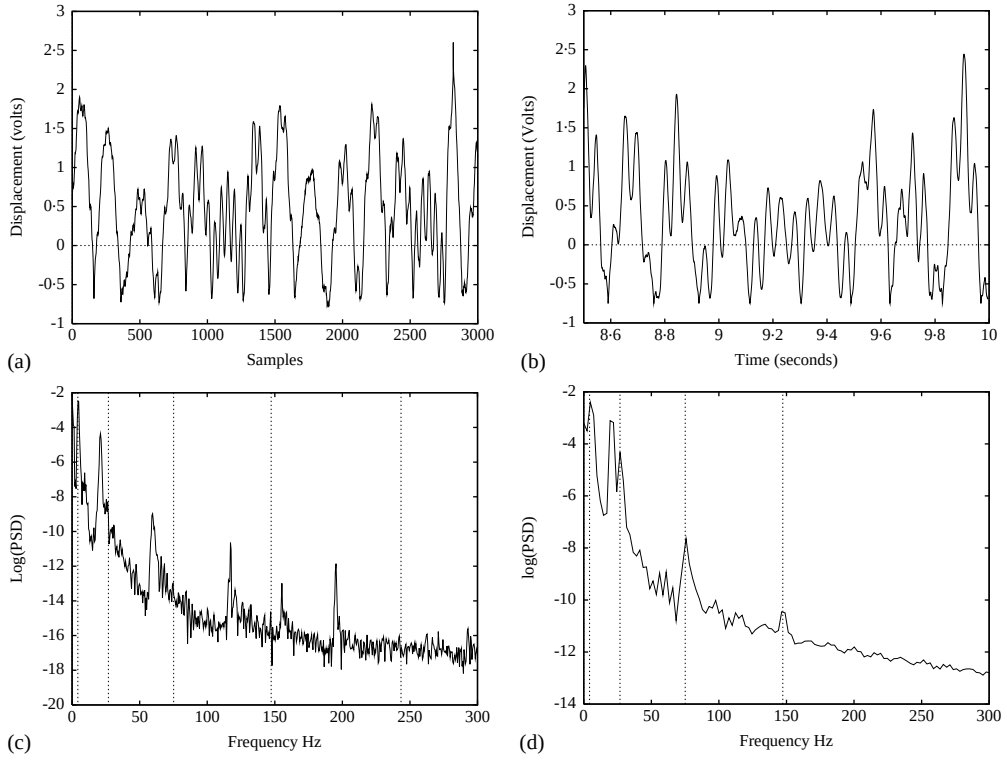

Figure 7. Impacting beam simulation: (a) Experimentally recorded signal for the beam and power spectrum sample rate 1000 sample/s, (b) numerical simulation, parameter values $u_s = -0{\cdot}7$, $N = 4$, $F = 0{\cdot}6$, $\Omega = 28{\cdot}3$, $\eta = 0{\cdot}005$, $r = 0{\cdot}8$, (c) power spectrum of signal shown in (a), vertical lines represent natural frequencies computed using classical beam theory and (d) numerically generated power spectrum.

caused by impacts, and therefore it is assumed that a four-mode model is sufficient to model the beam dynamics.

Thus, in Figure 7(b) a numerical simulation of the motion in Figure 7(a) is shown, using the non-smooth Galerkin approach, with $N = 4$. As with the non-impact result this simulation appears to give a good qualitative agreement with the experimental recorded time series in Figure 7(a). The power spectrum of the numerical simulation is shown in Figure 7(d). As would be expected, the main frequency components of this signal correspond to the first four computed natural frequencies. One significant additional frequency component occurs close to the second natural frequency; this can also be seen in the experimental spectrum, and is due to the forcing frequency at 20·8 Hz.

5.3. DIMENSIONALITY OF THE MODEL

In order to chose the number of modes to include in the modelling of the beam, the qualitative technique of examining the power spectrum of a recorded experimental time series has been used. By examining the spectrum, individual power spikes can be attributed to a particular modal contribution, and hence the number of modes for a model estimated. It is interesting therefore to consider the effect of underestimating the number of modes which contribute to the beam response.

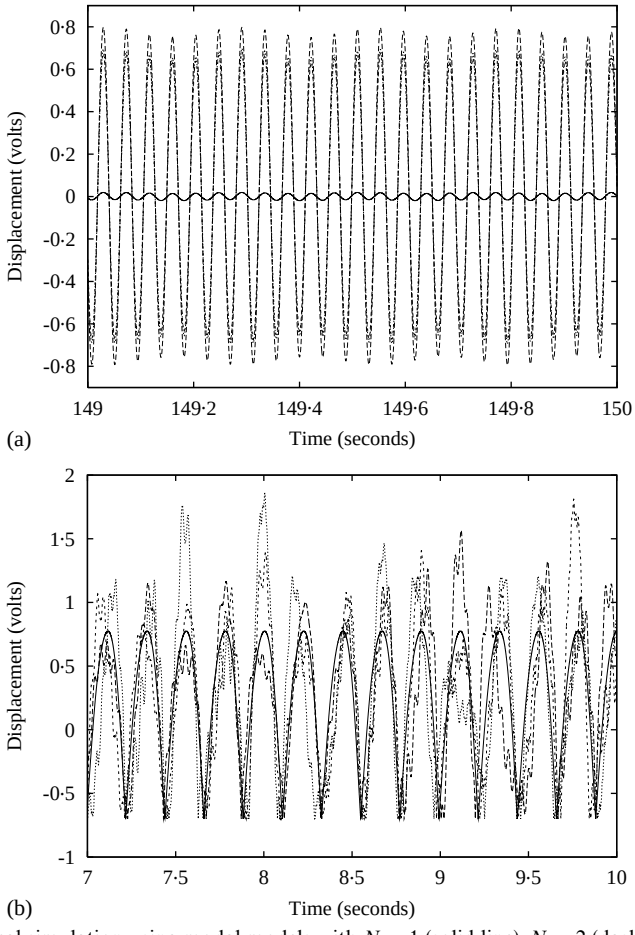

Figure 8. Numerical simulation using modal models with $N = 1$ (solid line), $N = 2$ (dashed line), $N = 3$ (short dashes) and $N = 4$ (dotted line). Parameter values $u_s = -0{\cdot}6$, $A = 0{\cdot}6$, $c = 0{\cdot}005$, $r = 0{\cdot}8$. (a) non-impacting $\Omega = 21{\cdot}0$ (b) vibro-impacting $\Omega = 28{\cdot}3$.

In Figure 8, numerical simulations for both the non-impacting case (a) and the vibro-impacting case (b) are presented with simulations using $N = 1, 2, 3$ and 4. For the non-impacting case, Figure 8(a), it can be seen that using a single-mode $N = 1$, the amplitude of response is significantly underestimated by the model. This is due to the fact that in this example the system is being forced close to the second natural frequency $f_2 \approx 21{\cdot}5$ Hz, and thus for a single-mode model with a resonance at $f_1 \approx 3{\cdot}8$ Hz the response to excitation at f_2 will be low amplitude. When the second mode is added, $N = 2$, as would be expected, the response becomes much closer to the experimental values, in fact, a slight overestimate. Finally there is very little difference between the solutions for $N = 3$ and 4, which gives a close qualitative agreement with experimental results.

For the vibro-impacting model, Figure 8(b), the single-mode solution $N = 1$ predicts a periodic vibro-impact solution. It is interesting to note that in this case the system is also being forced away from the first natural frequency but unlike the non-impact case the amplitude of response of the single-mode model is in good agreement with experimental data, Figure 7(a). The main difference is that the model is only capable of simulating periodic-type motion for a single harmonic forcing term, whereas the experimental system

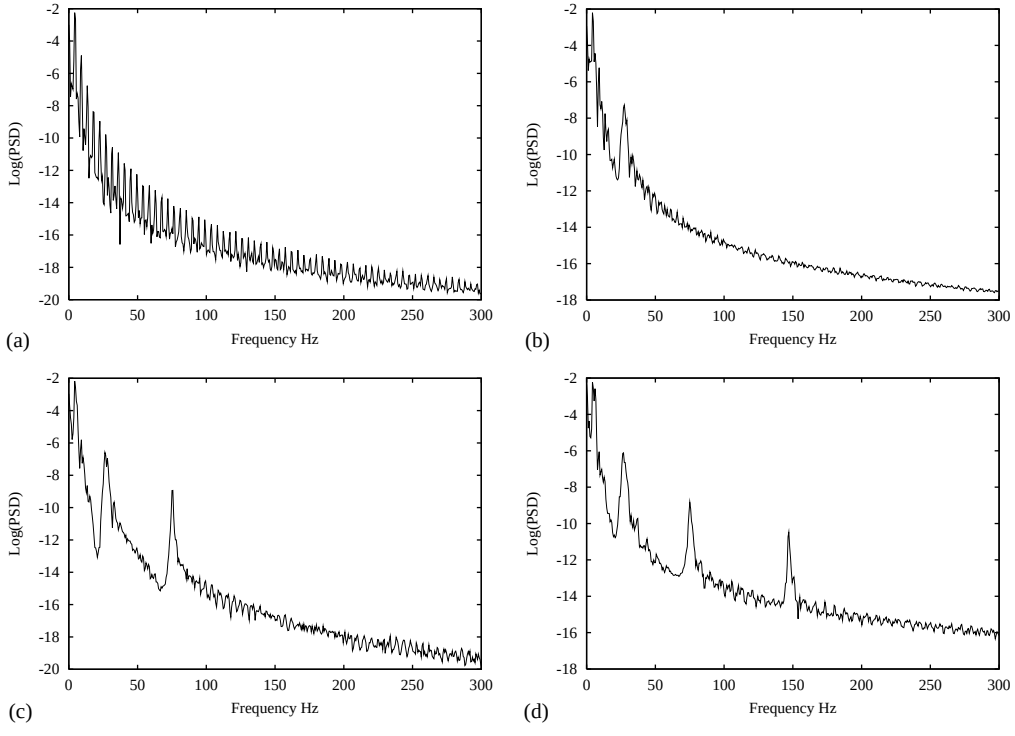

Figure 9. Power spectrum of the numerical simulations shown in Figure 8: (a) $N = 1$, (b) $N = 2$, (c) $N = 3$, and (d) $N = 4$.

appears to qualitatively exhibit a quasi-periodic-type response. Thus when additional modes are included in the model, $N = 2, 3, 4$ the quasi-periodic nature of the motion is represented in the response of the model. Note also that although each of the solutions $N = 2, 3, 4$ produces a qualitatively different response, the time of impact and maximum amplitudes are all approximately similar.

The power spectral densities for the numerical simulations in Figure 7 are shown in Figure 9. In Figure 9(a), a large number of harmonics are visible in the spectrum due to the sharply defined non-smooth discontinuity in the time series. In Figures 9(b)–(d) the harmonics are substantially reduced and the additional modal contributions, modes 2, 3 and 4, respectively, can be seen in the spectra.

5.4. BIFURCATION DIAGRAMS

Using the four-mode model for the beam, a measure of the beam displacement can be computed for a range of frequency values; for this analysis, the maximum minus the minimum displacement per forcing period is used. In this study, only frequency values close to the first resonance peak in the spectrum are considered which, for the experimental system, is $f_1 \approx 3{\cdot}2$ Hz. Figure 10(a), shows an experimentally recorded bifurcation diagram for the beam. In Figure 10(a) approximately 10 steady state readings from the beam tip at each frequency value were recorded, having first allowed the transients to decay. In this example, the impact stop was positioned at a displacement equivalent to approximately

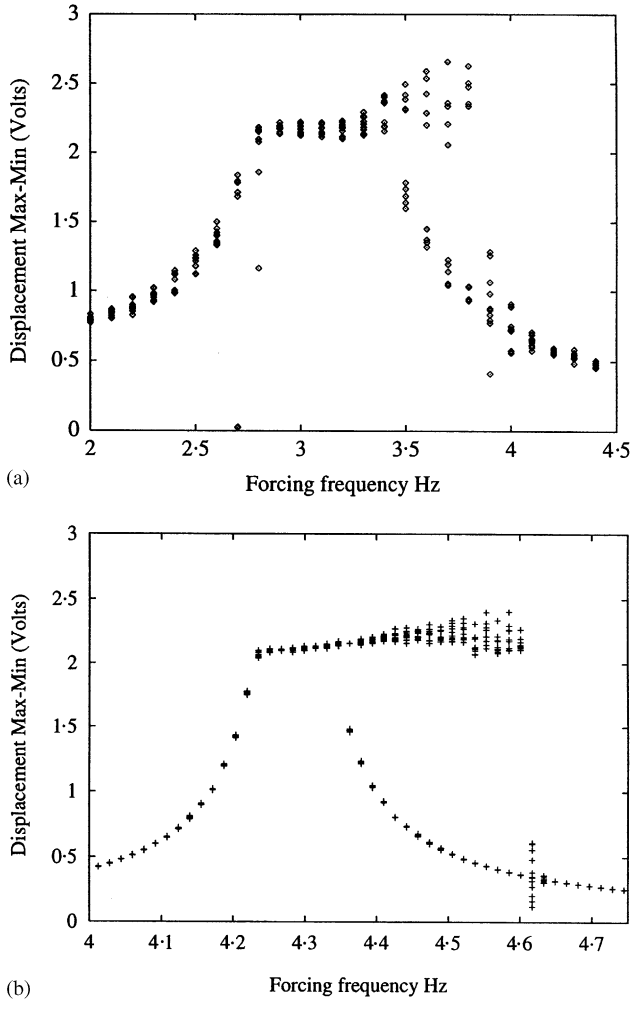

Figure 10. Flexible beam: (a) experimentally recorded bifurcation diagram (c) and (b) numerical simulation, parameter values $u_s = -1{\cdot}05$, $N = 4$, $A = 0{\cdot}1$, $c = 0{\cdot}0{\cdot}005$, $r = 0{\cdot}6$.

$-1{\cdot}05$ V. Therefore as the maximum minus minimum displacement is being plotted, the first grazing will occur at approximately 2.1 V. During these experiments, forcing amplitude was significantly reduced so that non-impacting resonance curves could also be recorded without excessively large beam vibrations.

In Figure 10(b), a numerically computed bifurcation diagram is shown for the first resonance peak in the four-mode model for which $f_1 \approx 4{\cdot}3$ Hz. It can be seen that the qualitative appearance of the two plots is similar, with a non-impacting behaviour below Max–Min $= 2{\cdot}1$ and hysteresis loop behaviour for frequencies greater than the non-impacting natural frequency indicating, as expected, hardening spring-type behaviour [7, 9]. Quantitatively, the numerical solution gives good agreement for Max–Min amplitude but is less accurate for the frequency values even after accounting for the approximately 1 Hz frequency shift between experiment and simulation. It appears that both the frequency scale and range have significant differences between experiment and simulation.

6. CONCLUSIONS

In this paper, non-smooth modelling techniques have been applied to continuous systems such as beams. Numerically computed simulations have been presented for flexible cantilever beam vibro-impact motion using this technique, which provide reasonable qualitative comparisons with experimentally recorded results within the parameter range studied.

The formation of the numerical model depends, in its current form, on the number of modes chosen being equal to the number of points considered on the beam. A further condition is that the point of impact must be included. This is a generalization of previous studies, where for a beam with a single point of impact the system was reduced to a single degree of freedom.

The impact process has been modelled using an instantaneous coefficient of restitution rule. The main limitation with this approach is that the impact time for flexible beams may not always be small, although allowance has been made for chatter and sticking motions. In systems where impact times are not short, the assumption of an instantaneous impact would not be valid and a different modelling approach would be required.

For engineering structures with high flexibility subject to non-smooth effects, such as impact and friction, multi-modal behaviour is a significant part of the dynamical behaviour. Single-degree-of-freedom models, although useful, do not fully capture this behaviour. The modelling process presented here provides a means of modelling the dynamics of continuous systems, with the inclusion of the higher dimensional dynamics.

REFERENCES

1. R. E. D. Bishop and D. C. Johnson 1960 *The Mechanics of Vibration*. Cambridge: Cambridge University Press.
2. L. Meirovitch 1967 *Analytical Methods in Vibration*. New York: McGraw-Hill.
3. S. P. Timoshenko, D. H. Young and W. Weaver Jr. 1974 *Vibration Problems in Engineering*. U.S.A.: Van Nostrand
4. A. Fathi and N. Popplewell 1994 *Journal of Sound and Vibration* **170**, 365–375. Improved approximations for a beam impacting a stop.
5. J. Wang and J. Kim 1996 *Journal of Sound and Vibration* **191**, 809–823. New analysis method for a thin beam impacting against a stop based on the full continuous model.
6. F. C. Moon and P. J. Holmes 1979 *Journal of Sound and Vibration* **65**, 275–296. A magnetoelastic strange attractor.
7. F. C. Moon and S. W. Shaw 1983 *International Journal of Non-Linear Mechanics* **18**, 465–477. Chaotic vibrations of a beam with non-linear boundary conditions.
8. S. W. Shaw 1985 *Journal of Sound and Vibration* **99**, 199–212. Forced vibrations of a beam with one-sided amplitude constraint: theory and experiment.
9. S. R. Bishop, M. G. Thompson and S. Foale 1996 *Proceedings of the Royal Society of London, Series A* **452**, 2579–2592. Prediction of period-1 impacts in a driven beam.
10. S. R. Bishop, D. J. Wagg and D. Xu 1998 *Chaos, Solitons and Fractals* **9**, 261–269. Use of control to maintain period-1 motions during wind-up or wind-down operations of an impacting driven beam.
11. T. Watanabe 1978 *Journal of Mechanical Design* **100**, 487–491. Forced vibration of continuous system with nonlinear boundary condition.
12. S. W. Shaw and P. J. Holmes 1983 *Journal of Sound and Vibration* **90**, 129–155. A periodically forced piecewise linear oscillator.
13. J. M. T. Thompson and R. Ghaffari 1982 *Physics Letters A* **91**, 5–8. Chaos after period doubling bifurcations in the resonance of an impact oscillator.
14. S. W. Shaw and P. J. Holmes 1983 *American Society of Mechanical Engineers Journal of Applied Mechanics* **50**, 849–857. A periodically forced impact oscillator with large dissipation.

15. A. B. NORDMARK 1991 *Journal of Sound and Vibration* **145**, 275–297. Non-periodic motion caused by grazing incidence in an impact oscillator.
16. S. R. BISHOP 1994 *Philosophical Transactions the Royal Society of London Series A* **347**, 347–351. Impact oscillators.
17. W. CHIN, E. OTT, H. E. NUSSE and C. GREBOGI 1994 *Physical Review E* **50**, 4427–4444. Grazing bifurcations in impact oscillators.
18. C. J. BUDD, F. DUX and F. CLIFFE 1995 *Journal of Sound and Vibration* **184**, 475–502. The effect of frequency and clearance variations on single degree of freedom impact oscillators.
19. M. H. FREDRIKSSON and A. B. NORDMARK 1997 *Proceedings of the Royal Society of London, Series A* **453**, 1261–1276. Bifurcations caused by grazing incidence in many degrees of freedom impact oscillators.
20. R. H. B. FEY, E. L. B. VAN DE VORST, D. H. VAN CAMPDEN, A. DE KRAKER, G. J. MEIJER and F. H. ASSINCK 1994 Chaos and bifurcations in a multi-dof beam system with nonlinear support. In *Nonlinearity and Chaos in Engineering Dynamics* (J. M. T. Thompson and S. R. Bishop, editors), pp. 125–139. Chichester: John Wiley; Chapter 9.
21. J. SHAW and S. W. SHAW 1989 *Journal of Applied Mechanics* **56**, 168–174. The onset of chaos in a two-degree of freedom impacting system.
22. J. P. CUSUMANO and B.-Y. BAI 1993 *Chaos, Solitons and Fractals* **3**, 515–536. Period-infinity periodic motions, chaos and spatial coherence in a 10 degree of freedom impact oscillator.
23. R. D. NEILSON and D. H. GONSALVES 1993 Chaotic motion of a rotor system with a bearing clearance. In *Applications of Fractals and Chaos* (A. J. Crilly, R. A. Earnshaw and H. Jones, editors), pp. 285–303. Berlin: Springer-Verlag.
24. D. J. WAGG and S. R. BISHOP 2001 *International Journal of Bifurcation and Chaos* **11**, 57–71. Chatter, sticking and chaotic impacting motion in a two-degree of freedom impact oscillator.
25. M. WIERCIGROCH and B. DE KRAKER, editors. 2000 *Applied Nonlinear Dynamics and Chaos of Mechanical Systems with Discontinuities*. Singapore: World Scientific Publishing.
26. J. P. CUSUMANO, M. T. SHARKADY and B. W. KIMBLE 1994 *Philosophical Transactions of the Royal Society of London Series A* **347**, 421–438. Experimental measurements of dimensionality and spatial coherence in the dynamics of a flexible-beam impact oscillator.
27. M. F. A. AZEEZ and A. F. VAKAKIS 2001 *Journal of Sound and Vibration* **240**, 859–889. Proper orthogonal decomposition (POD) of a class of vibroimpact oscillations.
28. P. METALLIDIS and S. NATSIAVAS 2000 *International Journal of Non-linear Mechanics* **35**, 675–690. Vibration of a continuous system with clearance and motion constraints.
29. Y. V. MIKHLIN and A. M. VOLOK 2000 *International Journal of Solids and Structures* **37**, 3403–3420. Solitary transversal waves and vibro-impact motions in infinite chains and rods.
30. E. EMACI, T. A. NAYFEY and A. F. VAKAKIS 1997 *Zeitschrift fur Angewandte Mathematik und Mechanik* (*ZAMM*) **77**, 527–541. Numerical and experimental study of nonlinear localization in a flexible structure with vibro-impacts.
31. M. F. A. AZEEZ and A. F. VAKAKIS 1999 *International Journal of Non-linear Mechanics* **34**, 415–435. Numerical and experimental analysis of a continuous overhung rotor undergoing vibro-impacts.
32. V. I. BABITSKY 1998 *Theory of Vibro-impact Systems and Applications*. Berlin, Heidelberg: Springer-Verlag.
33. D. J. WAGG, G. KARPODINIS and S. R. BISHOP 1999 *Journal of Sound and Vibration* **228**, 243–264. An experimental study of the impulse response of a vibro-impacting cantilever beam.
34. C. A. J. FLETCHER 1984 *Computational Galerkin Methods*. New York: Springer-Verlag.
35. R. D. BLEVINS 1979 *Formulas for Natural Frequency and Mode Shape*. New York: Van Nostrand Reinhold.
36. S. FOALE and S. R. BISHOP 1994 *Nonlinear Dynamics* **6**, 285–299. Transient response of a constrained beam subjected to narrow-band random excitation.
37. C. J. BUDD and F. DUX 1994 *Philosophical Transactions of the Royal Society of London, Series A* **347**, 365–389. Chattering and related behaviour in impact oscillators.
38. F. PFEIFFER and C. GLOCKER 1996 *Multibody Dynamics with Unilateral Contacts*. New York: John Wiley.